Hindawi
Journal of Food Biochemistry
Volume 2023, Article ID 6667315, 17 pages
https://doi.org/10.1155/2023/6667315

Research Article

Study on the Potential Mechanism of Traditional Marine Chinese Medicine Beishashen in Preventing Lung Injury Induced by Radiotherapy and Chemotherapy

Bin Yu,[1,2] **Maoru Wang**,[3] **Lina Jia**,[4] **Hui Xu**,[2] **Yuanying Zhu**,[2] **Yan Wu**,[2] **Ting Luo**,[2] **Yubing Zhou**,[2] **and Hong Ning**[1]

[1]*NHC Key Laboratory of Nuclear Technology Medical Transformation (Mianyang Central Hospital), Department of Pharmacy, Mianyang Central Hospital, Mianyang, Sichuan, China*
[2]*School of Pharmacy, Collaborative Innovation Center of Advanced Drug Delivery System and Biotech Drugs in Universities of Shandong, Key Laboratory of Molecular Pharmacology and Drug Evaluation, Yantai University, Yantai, Shandong, China*
[3]*Drug Dispensing Department, The Third Hospital of Mianyang, Sichuan Provincial Mental Health Center, Mianyang, Sichuan, China*
[4]*Department of Central Sterile Supply Department, Mianyang Central Hospital, Mianyang, Sichuan, China*

Correspondence should be addressed to Bin Yu; medicine2134@163.com

Received 23 July 2023; Revised 30 September 2023; Accepted 13 October 2023; Published 21 October 2023

Academic Editor: Nadica Maltar Strmečki

Lung injury after chemoradiotherapy is a common adverse reaction that is caused by radiation and chemotherapy drugs. Beishashen is a traditional marine Chinese medicine with multiple pharmacological properties. The previous research reported that it has a potential prevention effect on injuries caused by radiation and chemotherapy drugs, but the specific mechanism is unknown. Consequently, this study is based on bioinformatics and other methods, focusing on exploring the potential targets and molecular mechanisms of Beishashen in preventing lung injury after radiotherapy and chemotherapy. This study used network pharmacology methods to identify the bioactive compounds of Beishashen in order to better understand its therapeutic radiation-induced lung injury (RILI) and chemotherapy-induced lung injury (CILI) molecular mechanisms. We found that the role of Beishashen in preventing RILI and CILI involved several main pathways, especially the PI3K-AKT signaling pathway. PTGS2, PIK3CG, and RXRA were considered as key targets. Molecular docking and molecular dynamics showed good binding between the active ingredients and key targets, especially between alloisoimperatorin and RXRA. This study revealed the role of Beishashen in some potential regulating signal pathways in the treatment and prevention of RILI and CILI. Quercetin and alloisoimperatorin were the main active ingredients with low toxicity and can effectively bind with key targets. These findings provided important insights into the potential use of Beishashen for RILI and CILI.

1. Introduction

Malignant tumors remain one of the leading causes of death worldwide, and tumor prevention and treatment have increasingly become a major technological issue in the field of life and health and the healthcare industry [1]. Radiation therapy is an effective tool used in the treatment of tumors, but it can cause normal tissue damage, especially lung injury after radiotherapy for breast cancer, lung cancer, or other malignant tumors of the chest [2]. In addition, many patients undergo synchronous chemotherapy to enhance the antitumor efficacy of radiation, which can lead to the exacerbation of lung injury, known as chemotherapy-induced lung injury (CILI) [3, 4]. With an incidence rate of 10% to 40%, radiation-induced lung injury (RILI) is the most frequent and harmful side effect of radiotherapy for chest tumors. In severe cases, it can cause respiratory failure and endanger life, making it a key limiting factor for radiation

dose [5, 6]. The clinical manifestations of CILI generally include fever, cough, and difficulty breathing, and both cytotoxic and noncytotoxic drugs can cause lung injury [7]. Chemotherapy drugs are an important cause of drug-induced lung injury, accounting for about 10% of patients receiving chemotherapy [8]. Currently, the clinical treatment of both RILI and CILI mainly involves symptomatic treatment. However, pure antibacterial therapy is ineffective for RILI and CILI, and a large amount of glucocorticoids can alleviate early acute inflammatory reactions, but their efficacy in late-stage radiation-induced pulmonary fibrosis is not ideal, and they are accompanied by adverse reactions such as secondary infection, immunosuppression, and an increased risk of tumor metastasis or recurrence [9]. Cytotoxic drugs such as amifostine, interferon, ambroxol, and methotrexate also have certain clinical effects, but the many toxic side effects inherent in the drugs greatly limit their application, and their use can exacerbate or lead to exacerbation of lung injury [10–13]. Therefore, the exploration and discovery of drugs that have the effect of preventing and treating radiation and chemotherapy damage and their transformation into clinical applications has become a challenging issue that urgently needs to be addressed in the current field of cancer clinical practice.

Coasta-Glehnia-Root (Beishashen or Shashen) is the dry root of the Umbelliferae plant Glehnia littoralis Fr. Schmidt ex Miq. It benefits the stomach, nourishes the yin, and clears the lungs (this is a treatment method in traditional Chinese medicine that nourishes the negative fluid in the lungs, making it sufficient and achieving the goal of treating diseases), and stimulates fluid production. It is commonly used to treat lung heat and dry cough, cough and phlegm, stomach yin deficiency, heat disease, fluid injury, dry throat and thirst, etc [14]. It is mainly produced in coastal provinces of China, including Shandong, Liaoning, and Jiangsu provinces, as well as on beaches or beaches in South Korea, Japan, and the northwest of the United States. It is a traditional marine Chinese medicine in China, and current modern pharmacological research has found that Beishashen and its extracts have antioxidant, antitumor, anti-inflammatory, antibacterial, and neuroprotective effects [15–19]. In recent years, some scholars have found through data mining that Beishashen has potential therapeutic value in traditional Chinese medicine interventions for RILI, but their mechanisms of action in preventing and treating RILI and CILI have not been thoroughly studied [20]. In addition, the clinical efficacy of traditional Chinese medicine in treating lung injury caused by radiotherapy and chemotherapy has been improved through syndrome differentiation intervention, and traditional Chinese medicine has a potential utilization mechanism for the prevention and treatment of RILI and CILI [21, 22].

Therefore, our present study aims to explore the possible main active ingredients, key targets, and potential molecular mechanisms of traditional marine Chinese medicine Beishashen in the prevention and treatment of RILI and CILI. Meanwhile, we investigate the animal experimental studies and clinical application of Beishashen and related prescriptions for CILI or RILI. The findings of the present study would provide a theoretical reference and scientific basis for the screening of effective ingredients in Beishashen, the prevention and treatment of RILI and CILI, and the modernization of marine medicine research. Figure 1 displays the study's procedure.

2. Materials and Methods

This study will analyze the possible main active ingredients, key targets, and potential molecular mechanisms of Beishashen in preventing and treating RILI and CILI through network pharmacology, molecular docking, molecular dynamics, prediction of the pharmaceutical properties of active ingredients, quality analysis, and other methods and means.

2.1. Chemical Composition and Active Ingredients of Beishashen. The traditional Chinese medicine systems pharmacology database TCMSP was used to collect the active ingredients and targets of Beishashen, and to examine the retrieved ingredients' active ingredients. Oral bioavailability (OB) > 30% and drug similarity (DL) > 0.18 were the screening requirements [23]. After obtaining the active ingredients and corresponding targets of Beishashen, the target proteins were merged, deweighted, and then standardized using the UniPort protein database.

All active ingredients' chemical compositions of Beishashen are included in the TCMSP database. The TCMSP database also offers downloads of the appropriate chemical structures of the active substances that were obtained. In addition, a MOL2-format molecular structure file of the active ingredient was obtained for further use in molecular docking and molecular dynamics.

2.2. Acquisition of RILI and CILI Targets. The associated targets for RILI and CILI were searched using the GeneCards database and the Online Mendelian Inheritance in Man (OMIM) database. For instance, the relevant targets downloaded in databases were combined and then deduplicated to acquire the RILI relevant targets after "radiation-induced lung injury" was entered as a keyword in two databases. Only targets with relevant scores ≥10 were included in the GeneCards database, while all targets in the OMIM database were included. Following the use of R software, a Venn diagram of the Beishashen and RILI targets is drawn. Finally, the core targets of RILI were achieved. We also obtained CILI-related targets using the same procedure.

2.3. Construction of Protein-Protein Interaction. On the strings platform, the protein-protein interaction (PPI) network was built. The "Multiple Proteins" option was first chosen, after which the name lists for the primary targets were added, and "Homo sapiens" was added to the organism query. The PPI network diagram was eventually obtained after default values for other parameters were inserted.

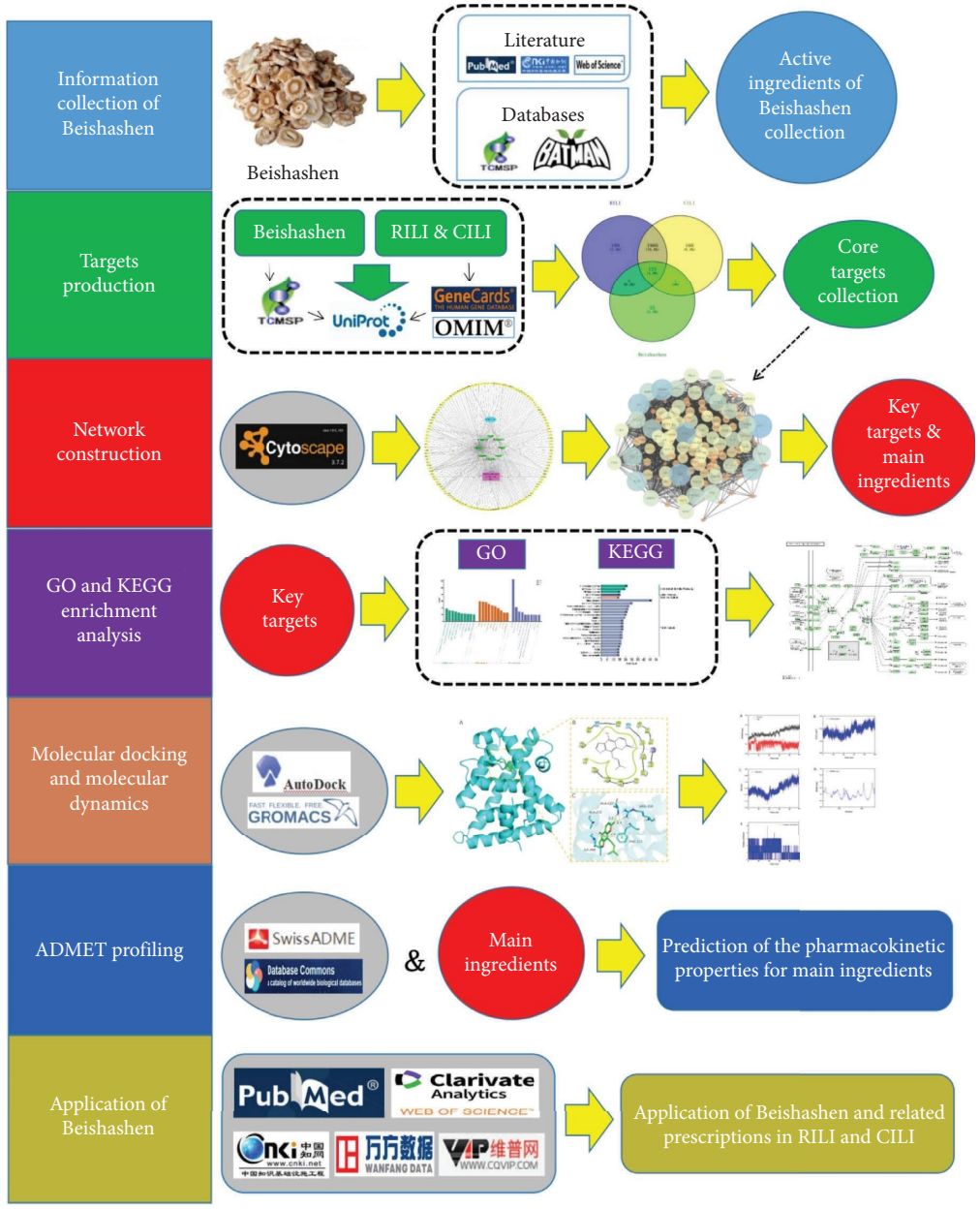

Figure 1: Graphical synopsis representation of this study.

2.4. Construction of Active Ingredient-Disease-Target Network. We created a visual network graph of the active ingredient-disease-target network using Cytoscape 3.7.2 software. Firstly, we input the obtained drugs, ingredients, diseases, and common targets into Cytoscape 3.7.2 software. Subsequently, the network analyzer in the Cytoscape plugin was used to determine the "network nodes" topological properties. These features included varying degrees of correlation, namely, degree, medium, and proximity. Besides, the five highest-assigned core targets were obtained based on degree values. Finally, the ingredient-disease-target network diagram was also generated during the aforementioned operation process.

2.5. KEGG Pathway Analysis and GO Functional Analysis. Understanding the main targets' functions and important pathways of Beishashen prevention and treatment for RILI and CILI was made easier by Gene Ontology (GO) function analysis and Kyoto Gene and Genome Encyclopedia (KEGG) pathway analysis. We input core targets into the DAVID platform to obtain GO functional examination of cellular components, biological processes, and molecular functions. Subsequently, the top 10 items with the highest counts for each item were utilized to create a histogram with a p value using R software; it was statistically significant when $p < 0.05$. Similarly, we also obtained the outcomes of

the DAVID platform's KEGG pathway analysis and drew a bar chart with the top 21 items with the highest count and p value; it was statistically significant when $p < 0.05$.

2.6. Molecular Docking. The molecular docking mechanism between the top five major targets in the degree ranking of the PPI network and the major five ingredients was verified using AutoDock software. The three-dimensional structures of the five target proteins were sourced from the RCSB PDB protein structure database, while the MOL2 file format of the active ingredients' structures were sourced from the TCMSP platform. In addition, the docking active site was located using the AutoDock plugin AutoGrid, and molecular docking was conducted to determine affinity. The lower the binding energy, the better the binding affinity between the target and the active ingredient was when we employed binding energy $\leq 5.0\ \text{kJ}\cdot\text{mol}^{-1}$ as a key molecule with better binding affinity to key targets [24]. Low-free binding energy docking data were visualized using the PyMOL program.

2.7. Molecular Dynamics. The molecular dynamics (MD) simulations were carried out by GROMACS 2020.3 software. The simulation box size was optimized with the distance between each atom of the protein and the box greater than 1.0 nm. Then, fill the box with water molecules based on a density of 1. To make the simulation system electrically neutral, the water molecules were replaced with Cl^- and Na^+ ions. Following the steepest descent method, energy optimization of 5.0×10^4 steps was performed to minimize the energy consumption of the entire system and, finally, to reduce the unreasonable contact or atom overlap in the entire system. After energy minimization, first-phase equilibration was performed with the NVT ensemble at 300 K for 100 ps to stabilize the temperature of the system. Second-phase equilibration was simulated with the NPT ensemble at 1 bar and 100 ps. The primary objective of the simulation is to optimize the interaction between the target protein and the solvent and ions so that the simulation system is fully preequilibrated. All MD simulations were performed for 100 ns under an isothermal and isostatic ensemble with a temperature of 300 K and a pressure of 1 atmosphere. The temperature and pressure were controlled by the V-rescale and Parrinello–Rahman methods, respectively, and the temperature and pressure coupling constants were 0.1 and 0.5 ps, respectively. Lennard–Jones function was used to calculate the Van der Waals force, and the nonbond truncation distance was set to 1.4 nm. The bond length of all atoms was constrained by the LINCS algorithm. The long-range electrostatic interaction was calculated by the particle Mesh-Ewald method with the Fourier spacing 0.16 nm.

2.8. ADMET Profiling. Drug research and development heavily depend on understanding chemical absorption, distribution, metabolism, excretion, and toxicity (ADMET). ADMET analysis helps to achieve possibly the best balance of properties required for drug discovery, which is both effective and safe [25]. In this regard, SWISS ADME and admetSAR were used to determine the physicochemical properties of the predicted ingredients. They were also used to predict the toxicity of potential active ingredients of Beishashen, such as acute oral toxicity, Ames mutagenesis, carcinogenic, hepatotoxicity, and nephrotoxicity.

2.9. Application of Beishashen and Related Prescriptions in RILI and CILI. In order to further understand the application of Beishashen and its prescriptions in RILI and CILI, we searched the relevant databases at home and abroad for their research reports on CILI and RILI in the past five years, and their research results were briefly introduced and summarized. Therefore, we used a combination of free words and subject words to search PubMed, Web of Science, China National Knowledge Infrastructure (CNKI), China Science and Technology Journal Database (VIP), and Wanfang databases from January 1, 2018, to October 1st, 2023. English search terms included "Beishashen," "Shashen," "Radiation," "Lung injury," "Chemotherapy." The research content is limited to clinical trials, clinical observational studies, clinical retrospective studies, and animal trials, but does not include reviews, pharmacokinetic studies, mechanism of action studies, meta-analysis, case reports, clinical guidelines, in vitro studies, etc. The language of the literature is limited to English or Chinese.

3. Results

3.1. Active Ingredients and Chemical Structure of Beishashen. Eight of the functional ingredients and 184 associated targets of Beishashen were acquired from TCMSP in accordance with the screening criteria previously established. Moreover, the predicted targets' name was transformed into gene names through the UniPort database. In addition, we also collected the chemical compositions of the eight main active ingredients of Beishashen through the TCMSP database, and their MOL2 files were also downloaded from the TCMSP database. Table 1 displays all of the facts in detail.

3.2. The Targets of RILI and CILI. GeneCards and the OMIM database were used to find the associated targets of RILI and CILI. While 452 associated targets were obtained from the OMIM database, 1927 related targets (relevance score 10) of RILI were obtained from the GeneCards database. 2297 RILI-related targets were discovered after the merging of two datasets and deduplication. The search and screening of CILI-related targets were also carried out according to the same process, with a total of 2264-related targets found from two databases. Besides, a Venn diagram was generated by using R software to identify the intersection of Beishashen active ingredient targets and the targets we obtained from RILI and CILI. We identified 129 core targets that were shared between the Beishashen active ingredients and RILI/CILI-related targets through this analysis. Figure 2 displays the outcomes.

Table 1: Active ingredients and related targets from Beishashen.

Mol ID	Molecule name	Targets	OB (%)	DL	MW
MOL001939	Alloisoimperatorin	PTGS1, AR, PTGS2, RXRA, HSP90, PIK3CG	34.80	0.22	270.30
MOL001941	Ammidin	F2, CHRM1, PTGS2, GABRA1, DPP4, PIK3CG, PRKACA, MAOB	34.55	0.22	270.30
MOL001942	Isoimperatorin	PTGS2	45.46	0.23	270.30
MOL001951	Bergaptin	KCNH2, SCN5A, PTGS2, ADRA1B, HSP90, PRKACA	41.3	0.42	338.43
MOL001956	Cnidilin	TR, CHRM1, SCN5A, PTGS2, RXRA, PTPN1, ADRB2, GABRG1, DPP4, HSP90, CHRNA7, PIK3CG	32.69	0.28	300.33
MOL000358	Beta-sitosterol	PGR, NCOA2, PTGS1, PTGS2, HSP90, PIK3CG, KCNH2, PPARG, DRD1, CHRM3, CHRM1, SCN5A, GABRA2, CHRM4, PDE3A, HTR2A, GABRA5, ADRA1A, GABRA3, CHRM2, ADRA1B, ADRB2, CHRNA2, SERT, OPRM1, GABRA1, CHRNA7, CAMC, BCL2, BAX, CASP9, NAPA, CASP3, CASP8, PRKCA, TGFB1, PON1, MAP2	36.91	0.75	414.79
MOL000449	Stigmasterol	PGR, MCR, NCOA2, ADH1C, IGHG1, RXRA, NCOA1, PTGS1, PTGS2, ADRA2A, SLC6A2, SLC6A3, ADRB2, AKR1B1, PLAU, LTA4H, MAOB, MAOA, PRKACA, CTRB1, CHRM3, CHRM1, ADRB1, SCN5A, HTR2A, ADRA1A, GABRA3, CHRM2, ADRA1B, GABRA1, CHRNA7	43.48	0.76	412.77
MOL000098	Quercetin	PTGS1, AR, PPARG, PTGS2, HSP90AB1, PIK3CG, NCOA2, DPP4, AR, TRY1, TOP2, TR, KCNH2, SCN5A, GAS6, ADRB2, MMP3, PRKACA, F7, NOS3, RXRA, ACHE, GABRA1, MAOB, RELA, AKT1, VEGFA, CCND1, BCL2, BCL2L1, FOS, CDK1, EIF6, BAX, CASP9, PLAU, MMP2, MMP9, MPK1, IL10, EGF, RBL1, TNF, NAPA, IL-6, CDKN2A, AHSA1, CASP3, TP53, ELK1, NFKBIA, POR, ODC1, XDH, CASP8, TOP1, RAF1, SOD, PRKCA, MMP1, HIF1A, STAT1, RUNX1T1, LOC103184504, CDC2, HELS89N, ERBB2, PPARG, ACC1, HMOX1, CYP3A4, CYP1A2, CAV1, MYC, F3, GJA1, CYP1A1, ICAM2, IL1B, CCL2, SELE, VCAM1, PTGER3, IL8, PRKCB, BIRC5, DUOX2, NOS3, HSPB1, TGFB1, SULT1E1, MGAM, IL2, NR1I2, CYP1B1, CCNB1, PLAT, THBD, SERPINE1, COL1A1, IFNG, ALOX5, PTEN, IL1A, MPO, TOP2A, NCF1, ABCG2, HAS2, GSTP1, NFE2L2, NQO1, PARP1, AHR, PSMD3, SLC2A4, COL3A1, GYRB, CXCL11, CXCL2, DCAF5, NR1I3, CHEK2, INSR, CLDN4, PPARA, PPARD, HSPB1, CRP, CXCL10, CHUK, SPP1, RUNX2, RASSF1, E2F1, E2F2, ACP3, CTSD, IGFBP3, IGF2, CD40LG, IRF1, ERBB3, PON1, DIO1, PCOLCE, NPEPPS, HK2, NKX31, RASA1, PRXC1A, GSTM2, GSTM1	46.43	0.28	302.25

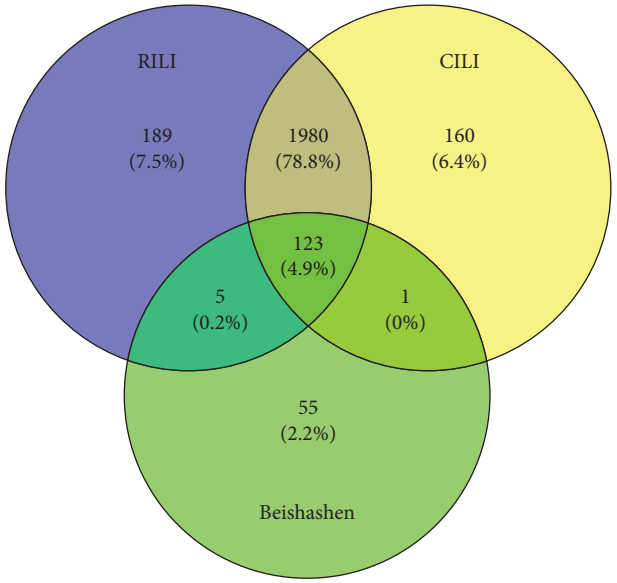

Figure 2: The Venn diagram between Beishashen, RILI, and CILI.

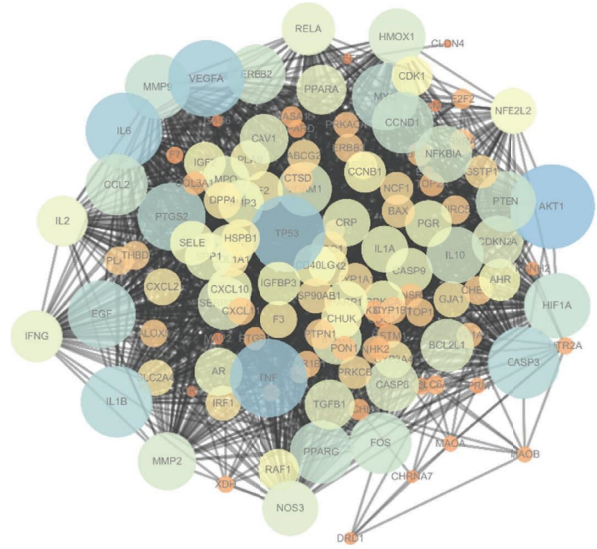

Figure 3: PPI network of core key targets.

3.3. PPI Network Construction. After incorporating 129 core targets into the string platform and selecting "Homo sapiens" to generate the PPI network, and subsequently, associated protein interaction relationships were acquired. Figure 3 displays the final result. Inherent 129 nodes and 2107 edges with a PPI enrichment p value of $1.0e-16$ were included in the PPI network map, where nodes stood for proteins and edges for the innate connections between them. The protein colors from orange to blue represent values from small to large. The PPI network map provided a visual representation of the protein interaction relationships among the core targets. The network can be further analyzed to identify key targets and pathways involved in the development and progression of RILI and CILI, which can help in the development of novel therapeutic strategies for these diseases.

3.4. Development of the Active Ingredient-Disease-Target Network. The network diagram of Beishashen-ingredient-target-RILI and CILI was constructed by Cytoscape 3.7.2 software, as shown in Figure 4. The network revealed numerous interactions between active ingredients and key targets, suggesting that Beishashen can prevent and counteract RILI and CILI through multitarget and multipathway synergistic interactions. Five primary ingredients of Beishashen and five important targets were examined using the Network Analyzer of the Cytoscape 3.7.2 software. The five main active ingredients were quercetin, beta-sitosterol, stigmasterol, cnidilin, and alloisoimperatorin, while the five key targets were prostglandinendoperoxide synthase 2 (PTGS2), sodium channel protein type 5 subunit alpha (SCN5A), phosphatidylinositol-4,5-bisphosphate 3-kinase catalytic subunit gamma (PIK3CG), prostglandinendoperoxide synthase 1 (PTGS1), and retinoic acid receptor RXR-alpha (RXRA).

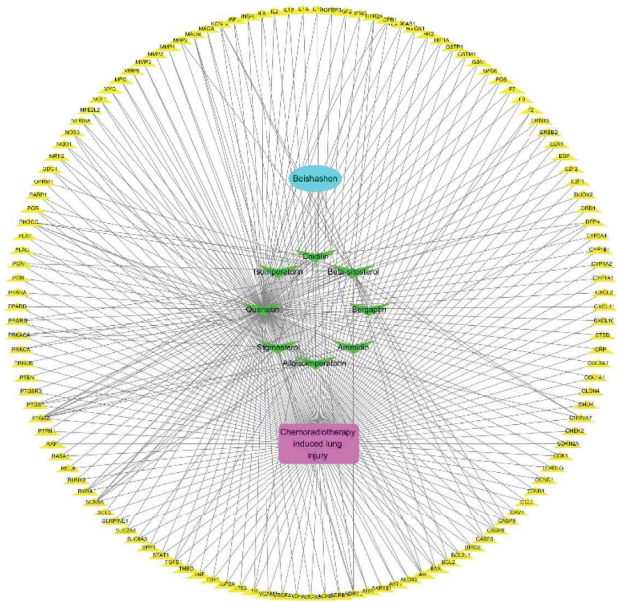

Figure 4: Drug-ingredient-target-disease network diagram.

3.5. Analysis of GO and KEGG Enrichment. The primary Beishashen targets for the prevention and treatment of RILI and CILI were subjected to GO enrichment analysis using the DAVID platform, and a total of 734 enriched GO entries with <0.05 were obtained. There were 55 cellular components, 568 biological activities, and 111 molecular functions. The GO enrichment analysis histogram is depicted in Figure 5 and was created using the top ten values of each count value. The results indicated that the main targets were mainly involved in biological processes such as positive regulation of translation from the RNA polymerase II

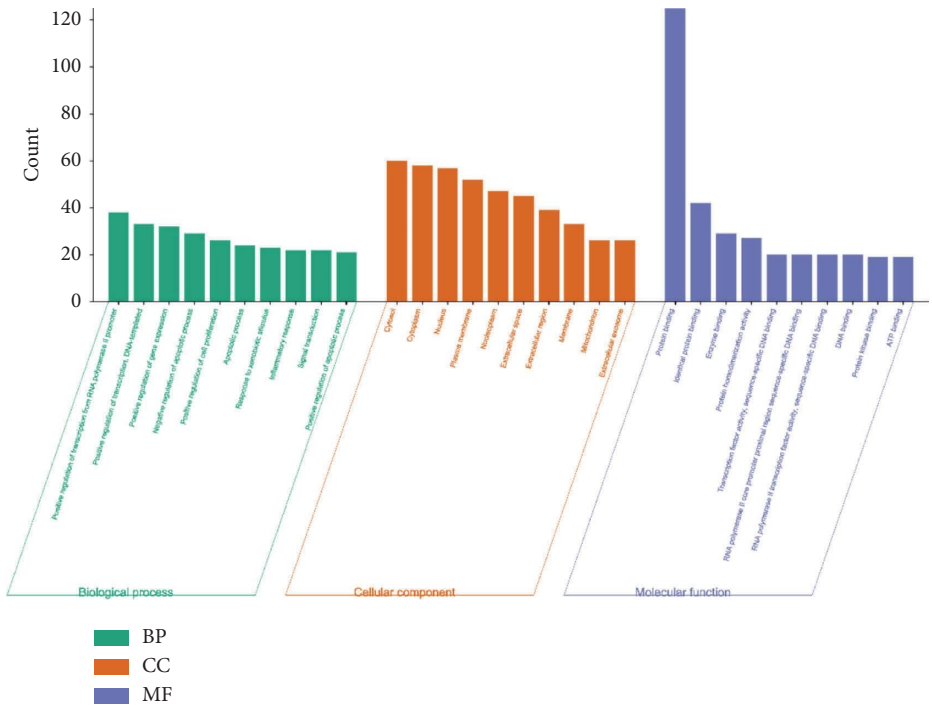

Figure 5: GO functional enrichment analysis.

promoter, positive regulation of translation, positive regulation of gene expression, negative regulation of the apoptotic process, DNA-templated, and positive regulation of cell promotion. They were distributed in the cyclosol, cycloplast, nucleus, plasma membrane, and nucleoplast. They also had molecular functions such as protein binding, identifying protein binding, enzyme binding, protein normalization activity, transcription factor activity, and sequence-specific DNA binding.

Similar to the above analysis, key targets were subjected to KEGG pathway enrichment analysis using the DAVID platform and R software, and the top 25 with the highest count value were chosen for bar chart display. The result was shown in Figure 6. The main signal pathways involved include the PI3K-AKT signaling pathway, the AGE-RAGE signaling pathway in diabetic applications, the MAPK signaling pathway, the TNF signaling pathway, and the IL-17 signaling pathway. The PI3K-AKT signaling pathway can be seen in Figure 7.

3.6. Molecular Docking Results. We used molecular docking to compare the five Beishashen active ingredients (alloisoimperatorin, quercetin, cnidilin, stigmasterol, and beta-sitosterol) and five core targets (RXRA, PIK3CG, SCN5A, PTGS1, and PTGS2), respectively. The outcomes of molecular docking demonstrated that each of the five ingredients had strong interactions with five target proteins and a high degree of matching, and all of the binding energy scores fell below $-6.0\,\text{kJ}\cdot\text{mol}^{-1}$. To determine the binding mode of the compound and target, we used Pymol2.1 software to view the compounds created by docking them with the targets. The amino acid residues that the molecule mixes with the target pocket are also easily visible, depending on the binding mode. Among them, alloisoimperatorin had the highest binding energy with RXRA and PIK3CG, and both were less than $-9.0\,\text{kJ}\cdot\text{mol}^{-1}$. In addition, the results also showed that the amino acid residues of alloisoimperatorin interacting with the active site of RXRA included ASN-306, ALA-327, ARG-316, etc. In addition, alloisoimperatorin has a significant degree of hydrophobicity and is capable of forming a potent hydrophobic contact with the RXRA (TRP-305, LEU-436, LEU309, VAL-342, ILE-345, ILE324, PHE313, PHE-346, CYS432, VAL-349, ILE-268, LEU326, ALA-271, and ALA-272) active site amino acids, which is crucial for stabilizing small molecules in protein cavities. Table 2 displays the outcomes.

3.7. Molecular Dynamics. The outcomes of molecular docking showed that the RXRA and alloisoimperatorin complex had the highest binding energy value in its entirety to investigate the interaction mode between the key protein RXRA and the core ingredient alloisoimperatorin at a molecular level. Based on the outcomes of the molecular docking, we ran molecular dynamics simulations. The root mean square deviation (RMSD) curve of the protein represented the fluctuation of RXRA conformation at different times. From Figure 8(a), it is apparent that during the initial stage of the molecular dynamics simulation (0–100 ns), the ligand RMSD value changed slightly while the protein RMSD value made a slight change. However, after 80 ns, the protein-ligand simulation system achieved equilibrium between the protein and ligand, and the protein RMSD value was greater than the ligand RMSD value, indicating that the

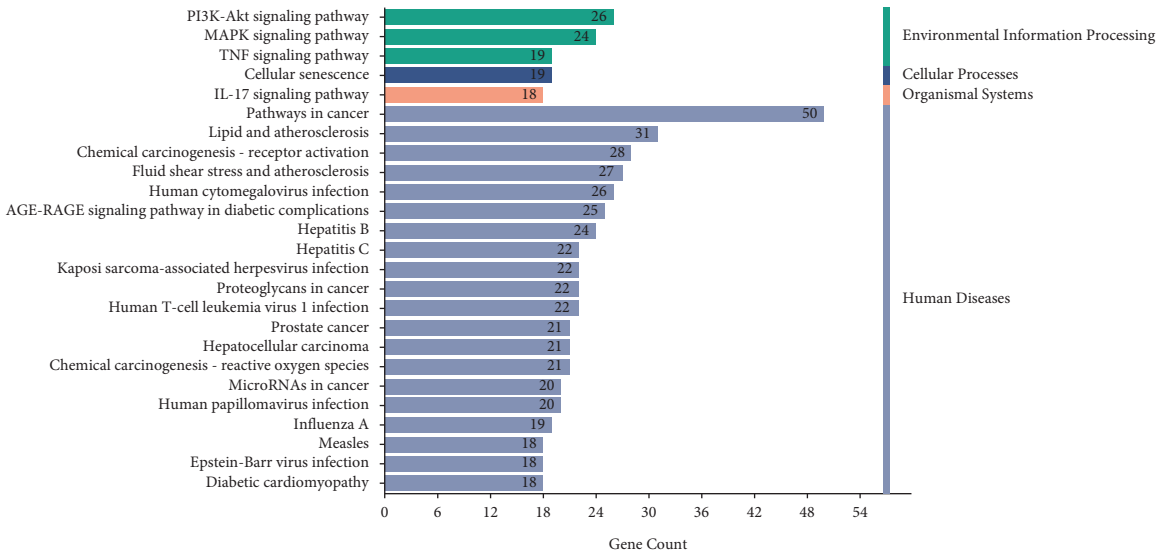

Figure 6: KEGG pathway enrichment analysis.

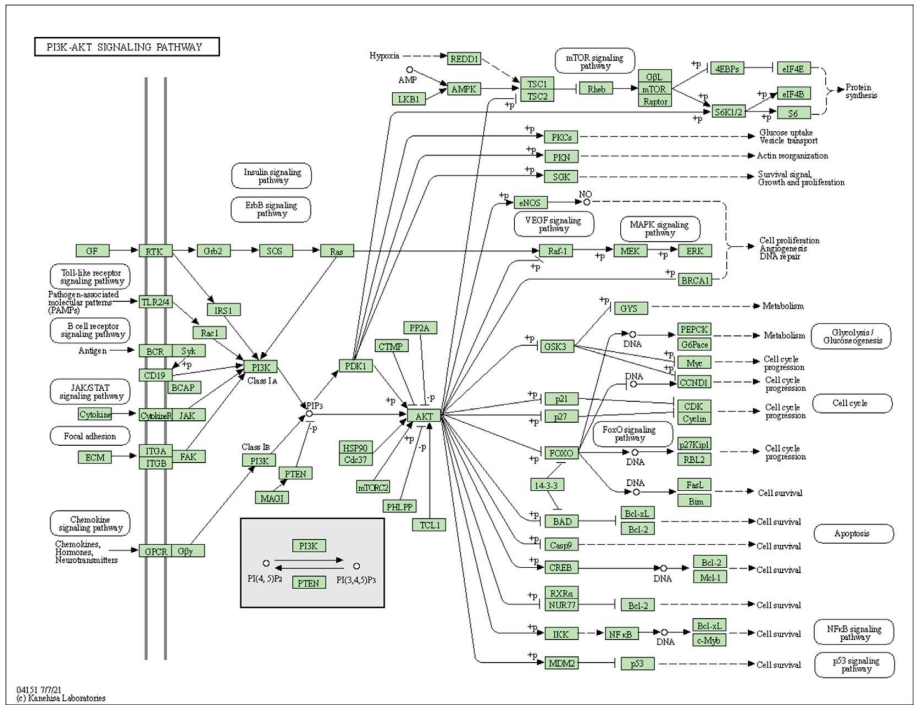

Figure 7: PI3K-AKT signaling pathway.

protein fluctuations were greater than the ligand fluctuations. The solvent accessible surface areas (SASA) were calculated by considering the interaction between van der Waals force and solvent molecules. The solvent accessible surface area of the protein decreases with an increase in protein compactness, so the change of SASA can predict the change in protein structure (Figure 8(b)). As seen in Figure 8(b), the protein-ligand complex's SASA values showed an upward trend during the simulation of protein-ligand recombination, indicating a decline in protein compactness. In addition, the radius of gyration (Rg) in Figure 8(c) also indicated that the Rg value and SASA value of the protein showed the same trend throughout the composite molecular dynamics simulation process, further signaling alterations to the protein-ligand system's structure.

We calculated the binding energy of all protein-ligand complexes in the equilibrium phase using the gmx_mmpbsa script to explain the interaction energy between the ligand and receptor. The entire binding energy was split into four separate components for the MMPBSA application: electrostatic interaction, van der Waals interaction, polar solvation, and nonpolar solvation interaction. Table 3 displays

Table 2: The molecular docking results.

Target	PDB ID	Active ingredients	Affinity (kJ·mol^{-1})	Best-docked complex (3D) and (2D)
PTGS2	5F1A	Quercetin	−8.71	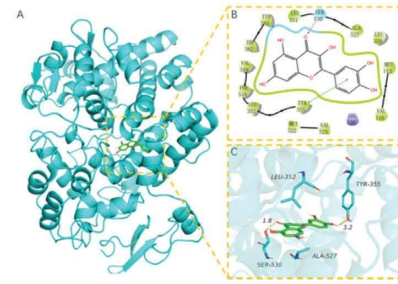
		Beta-sitosterol	−6.57	
		Stigmasterol	−6.79	
		Cnidilin	−6.83	
		Alloisoimperatorin	−7.04	
PIK3CG	4ANV	Quercetin	−7.71	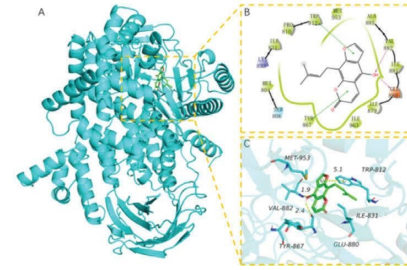
		Beta-sitosterol	−6.96	
		Stigmasterol	−7.18	
		Cnidilin	−7.71	
		Alloisoimperatorin	−9.10	
SCN5A	4JQ0	Quercetin	−7.53	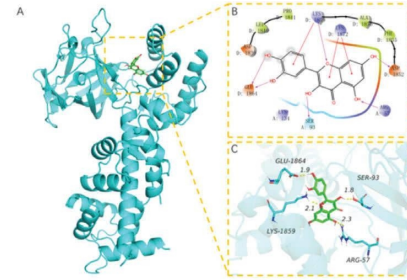
		Beta-sitosterol	−6.41	
		Stigmasterol	−6.10	
		Cnidilin	−6.90	
		Alloisoimperatorin	−7.16	
PTGS1	6Y3C	Quercetin	−7.68	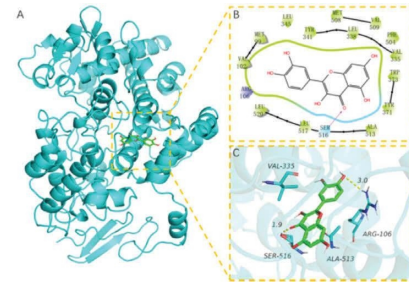
		Beta-sitosterol	−6.93	
		Stigmasterol	−6.56	
		Cnidilin	−7.38	
		Alloisoimperatorin	−7.16	
RXRA	4K4J	Quercetin	−8.68	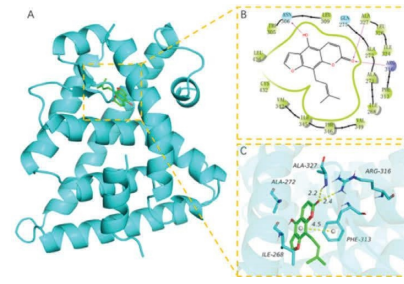
		Beta-sitosterol	−7.08	
		Stigmasterol	−7.21	
		Cnidilin	−7.76	
		Alloisoimperatorin	−9.32	

Note. A is the 3D structure of complex, B is the 2D binding mode of complex, C is the 3D binding mode of complex.

the findings of the protein and ligand's binding energy. The binding energy was negative in the protein-ligand complex system, indicating that it participated in the binding of the protein ligand. The protein's and the ligand's respective binding free energies were −23.437 kJ·mol^{-1}.

3.8. ADMET Profiling. Evaluation of the absorption, distribution, metabolism, and excretion (ADME) of various monomer components is necessary for the continued research and use of active ingredients in traditional Chinese medicine. Various criteria are used to evaluate a large

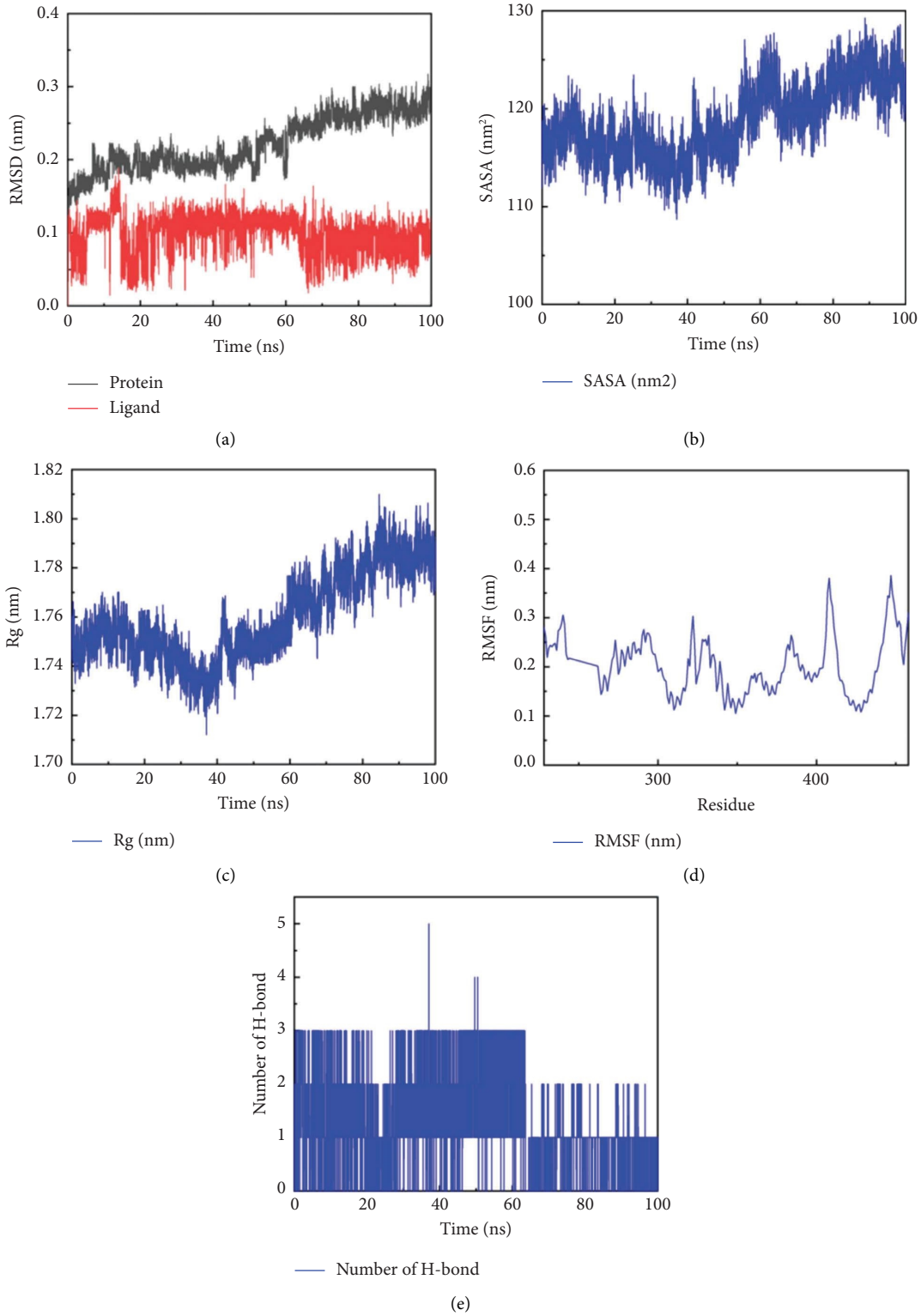

Figure 8: The stability results from RXRA-alloisoimperatorin complex by MD simulations at 100 ns trajectory. (a) Protein RMSD and ligand RMSD with time frame in 100 ns; (b) simulation of protein-ligand complex process: changes in protein SASA in 100 ns; (c) simulation of protein-ligand complexation process: changes in Rg of protein in 100 ns; (d) simulation of protein-ligand complexation process: changes in protein RMSF in 100 ns; (e) changes in hydrogen bond numbers within 100 ns during protein-ligand recombination simulation process.

Table 3: Protein ligand MMPBSA analysis.

Energy	EGFR (kJ·mol^{-1})
Van der Waals energy	−130.173
Electrostatic energy	−25.213
Polar solvation energy	131.573
Nonpolar solvation energy	−19.045
Total binding energy	−42.858
TΔS	19.421
Total binding free energy	−23.437

number of molecular structures and properties to guide the selection of drugs that are most likely to be useful to patients. ADME analysis was conducted using the SWISS ADME database and the admetSAR database, and the results showed that all ingredients had satisfactory pharmacokinetic properties (Table 4). The ADMET spectrum analysis results revealed that some main active ingredients had slight toxic side effects in their pharmacokinetic properties, while others also had liver or kidney toxicity. Quercetin had the least toxic side effects, and there was no liver or kidney toxicity, while cnidilin had more toxic side effects. The ADME characteristics of key active ingredients in different models, such as BBB permeant, P-gp substrate, CYP1A2 inhibitor, CYP2C19 inhibitor, and CYP2D6 inhibitor, had shown positive results in some potential ingredients, indicating their ability to serve as candidate drugs. Some compounds, such as quercetin and alloisoimperatorin, can be used as good candidate drugs for preclinical trials.

3.9. The Application of Beishashen and Its Related Prescriptions in RILI and CILI. According to our search conditions and requirements, a total of 10 articles about the application of the Beishashen prescription in clinical and animal experiments were included in the past 5 years, including 1 English paper and 9 Chinese papers. There is no research report on the use of Beishashen alone in recent 5 years. Beishashen is mostly studied in RILI and CILI in the form of traditional Chinese medicine prescriptions. In addition, there are 5 reports on the application of "Beishashen Maidong Decoction" as a research object in radiation pneumonia and lung injury; two articles reported the application of "Beishashen Jiegeng Decoction" as a research object in acute radiation-induced lung injury and radiation pneumonitis. The detailed results are shown in Table 5.

4. Discussion

The purpose of this work was to examine the probable mechanisms of Beishashen in the prevention and treatment of RILI and CILI using bioinformatics. Firstly, this work used the database to identify relevant targets for RILI and CILI after screening the active components and associated targets of Beishashen. The intersection targets were obtained through a Venn diagram. The team next built the active ingredient-disease-target network, performing enrichment analysis on the key targets. Based on the degree value, we identified five main active ingredients and five main action targets. These five active ingredients can successfully attach to those five important targets, with quercetin and RXRA having the highest binding energies. Finally, the study predicted the pharmacokinetic characteristics of these five active ingredients, particularly their toxicity, and provided a brief explanation.

Among the five main active ingredients of Beishashen, stigmasterol, cnidilin, and alloisohyperperorin have not been reported in clinical research, animal experimental, or reviews related to their prevention and treatment of RILI and CILI. However, stigmasterol was mentioned in a network pharmacology article on adjuvant treatment of pneumonia and was discovered as a major component of the Feilike mixture [36]. A popular phytosterol found in traditional Chinese medicine called beta-sitosterol has been shown to have anti-inflammatory and antioxidant properties. At present, it has not been found to have a clear therapeutic effect in RILI and CILI, but some scholars have found that it can improve the proinflammatory reaction and acute lung injury induced by influenza A virus in mice, as well as improve the lung histopathology injury and reduce the level of inflammatory factors [37]. Quercetin is the most abundant dietary flavonoid found in various plants and foods, with strong anti-inflammatory and antioxidant properties [38]. Some researchers used quercetin as an intervention drug to preprotect RILI model-injured mice and found that in hematoxylin and eosin staining, the radiation control group showed more severe lung injury than the quercetin group [39]. Immunohistochemistry and Western blotting results also revealed that, in contrast to the radiation control group, NF-B expression levels were reduced following quercetin intervention while NF-B inhibitor expression levels rose. In the radiation plus quercetin injection group, there were fewer inflammatory cells that were JNK/SAPK, p38, and p44/p42 positive ($p < 0.05$). Finally, they hypothesized that quercetin might inhibit NF-B and MAPK, which would protect mice's lungs from radiation. Meanwhile, Liu et al. also reckoned that the quercetin liposomes can prevent radiation-induced acute pneumonia and advanced fibrosis by reducing oxidative damage [40]. Quercetin-3-rutinoside is a potential therapeutic agent that can alleviate radiation-induced lung injury in planned or unplanned radiation exposure situations [41]. Although quercetin had certain protective effects and good therapeutic effects on lung injury caused by lipopolysaccharides, pneumolysin, bleomycin, paraquat, cigarette smoke, and even hyperoxia, there were few studies and reports on its use in CILI [42–47]. Therefore, more investigation is required to determine whether quercetin protects against the lung damage brought on by chemotherapy medicines.

For decades, it has been well established that radiation produces reactive oxygen species (ROS) [8]. However, chemotherapy, like radiotherapy, may induce endogenous production of ROS and nitric oxide by immune cells and some nonimmune cells (such as fibroblasts and endothelial cells) [48]. After inhaling anticancer medications, the primary sources of ROS produced are cyclooxygenase-2 (PTGS2, also known as COX-2) and the mitochondrial cellular respiration system. ROS overexpression increases with the expression of PTGS2, leading to cell apoptosis,

Table 4: ADMET profiling results of active ingredients.

Ingredients	Quercetin	Beta-sitosterol	Stigmasterol	Cnidilin	Alloisoimperatorin
GI absorption	High	Low	Low	High	High
BBB permeant	No	No	No	Yes	Yes
P-gp substrate	Yes	No	No	No	Yes
CYP1A2 inhibitor	Yes	No	No	Yes	Yes
CYP2C19 inhibitor	No	No	Yes	Yes	No
CYP2C9 inhibitor	No	No	No	No	No
CYP2D6 inhibitor	Yes	No	No	No	No
CYP3A4 inhibitor	No	No	No	No	No
Toxicity					
Acute oral toxicity	III	I	I	III	III
Ames mutagenesis	In-active	In-active	In-active	Active	In-active
Carcinogenicity	In-active	In-active	In-active	In-active	In-active
Hepatotoxicity	In-active	Active	Active	Active	Active
Nephrotoxicity	In-active	In-active	In-active	Active	In-active

necrosis, and aging, leading to inflammation and the release of profibrotic cytokines, ultimately leading to lung injury. In addition, Drishya et al. also intervened in radiation-induced pneumonia and pulmonary fibrosis through subcutaneous dry fruits (MEAS), and in immunohistochemical analysis, it revealed the significant potential of MEAS in reducing radiation-induced increased pulmonary PTGS2 expression, leading to a decrease in radiation-induced pulmonary fibrosis [49]. Li et al. found that PIK3CG is more likely a potential gene that promotes radiochemotherapy sensitivity, and there are currently no research reports on its protective effect after chemotherapy injury [50]. Besides, there also exist no relevant research reports or reviews on the key targets (SCN5A, PTGS1, and RXRA) in RILI or CILI in recent years. In enrichment analysis, we found that the main active ingredients of Beishashen can play a role through PI3K-AKT, AGE-RAGE in diabetic applications, MAPK, TNF, and IL-17 signaling pathways. The PI3K-AKT signaling pathway is the most important signaling pathway, which is consistent with the research results of other researchers [18, 51]. Moreover, Gong et al. demonstrated that ononin can regulate the antitumor effect of apoptosis in non-small-cell lung cancer cells by inhibiting the PI3K/AKT/mTOR pathway in animal experiments and can reduce the hepatorenal toxicity caused by paclitaxel [52]. Besides, a clinical study had shown that genetic variations in the PI3K-AKT pathway are significantly associated with ≥3 levels of radiation pneumonia, which can serve as a predictive indicator for severe radiation pneumonia before radiotherapy [53]. As shown in Figure 7, the MAPK signaling pathway is also regulated by the PI3K-AKT signaling pathway, so it may also be involved in the prevention and treatment mechanisms of RILI and CILI. This is also consistent with the research results of Arora and Xu et al. [54, 55]. Meanwhile, the TNF signaling pathway and the IL-7 signaling pathway, as classic pathways of inflammatory response, also play important roles in RILI and CILI [55, 56].

With respect to molecular docking and molecular dynamics, the five main active ingredients of Beishashen can bind to key targets, and their binding with energy is lower. Among them, the combination of alloisoimperatorin and RXRA is the best. In the further molecular dynamics simulation, we discovered that alloisoimperatorin and RXRA have a negative binding energy in the protein-ligand complex system, indicating that it is conducive to protein-ligand binding. The binding free energy of alloisoimperatorin and RXRA is $-23.437\ \mathrm{kJ{\cdot}mol^{-1}}$, and there also exist hydrogen bonding interactions between alloisoimperatorin and RXRA, with an average number of hydrogen bonds of 1.39, showing that their binding is relatively tight. In addition, we also predicted the pharmacokinetic properties of these five main active ingredients. According to the results of Table 4, quercetin, dnidilin, and alloisoimperatorin had an acute oral toxicity level of III, which is relatively low in toxicity. However, Cnidilin may have potential Ames mutagenesis, hepatotoxicity, and nephrotoxicity. Beta-sitosterol and stigmasterol had a level I acute oral toxicity, but no Ames mutagenesis, hepatotoxicity, and nephrotoxicity. Furthermore, these ingredients had no inhibitory effects on CYP2C19 and CYP3A4, but may have had potential inhibitory effects on other liver drug enzymes. At present, the traditional Chinese medicine prescription based on Beishashen has been applied in animal and clinical research, especially in the treatment and protection of radiation pneumonitis, which has achieved good curative effect, decreased inflammatory factors, and the adverse reactions of patients. However, Beishashen has not been used alone for the time being. Therefore, Beishashen is mostly used in the form of prescriptions in the current clinical research and has achieved good results. In summary, quercetin and alloisoimperatorin may be reliable alternative substances for RILI or CILI prevention and treatment, but further experimental verification is also needed. More importantly, we must recognize that although bioinformatics analysis relies on public databases, the data information is imperfect and requires ongoing improvement. Furthermore, this study also overlooked the effects of Beishashen from different regions and the content and concentration of active ingredients on RILI and CILI because only a specific number of medicines can effectively reach the target place. As a result, more confirmation and verification of the research's findings are required.

Table 5: The application of Beishashen and related formulas in RILI and CILI in the past 5 years.

Author	Name of drug or prescription	Formulation of the prescription	Major findings	Disease	Study types
Yang and Zhou [26]	Shashen-Maidong decoction	Coastal-Glehnia-root (Shashen) 18 g, Phyllostachys offcinalis (Houpo) 12 g, Ophiopogon japonicus (Maidong) 18 g, snake gourd root 9 g, lentils 9 g, mulberry leaf 9 g, liquorice 6 g, wolferry root-bar 18 g	↑IFN-γ, ↓IL-4, ↑immune function	Radiation pneumonia	Rats study
Qi et al. [27]	Shashen Jiegeng decoction	Beishashen 30 g, Balloon flower (Jiegeng) 10 g, Cortex Lycii 10 g, Peach seed (Taoren) 10 g, Fragrant solomon seal rhizome (Yuzhu) 10 g, Maidong 15 g, Lily (Baihe) 15 g, Hyacinth bean (Biandou) 15 g, Mulberry leaf (Sangye) 10 g, Raw licorice (Shenggancao) 6 g, Almond (Xingren) 10 g, Trichosanthin (Tianhuafen) 15 g	Degeneration of bronchial epithelial cells in the Chinese medicine group was not obvious, the alveolar wall was slightly widened, a small amount of inflammatory cell infiltration, semiquantitative scores of alveolitis were significantly reduced	Acute radiation-induced lung injury	Rats study
Wu et al. [28]	Shashen-Maidong decoction	Beishashen 9 g, Yuzhu 10 g, Gancao 3 g, Sangye 4.5 g, Maidong 9 g, Biandou 4.5 g, Pollen (Huafen) 4.5 g	↓IL-6, ↓TNF-α, ↓incidence of adverse reactions, ↑quality of life scale	Lung injury	Clinical study
Wu et al. [29]	Shashen Jiegeng decoction	Beishashen 30 g, Jiegeng 10 g, Taoren 10 g, Yuzhu 10 g, Digupi 10 g, Maidong 15 g, Baihe 15 g, Tianhuafen 15 g, Biandou 10 g, Sangye 10 g, Xingren 10 g, Gancao 6 g	↓IL-6, ↓TNF-α, ↓TGF-β_1, ↑total effective rate, ↑FEV1, ↑FVC, ↑FEV1/FVC, ↑VC, ↑carbon monoxide diffusing capacity (DLCO)	Radiation pneumonia	Clinical observation study
Li et al. [30]	Shashen Maidong decoction	Beishashen 15 g, Yuzhu 10 g, Maidong 15 g, Biandou 10 g, Gancao 6 g, Tianhuafen 10 g, Sangye 10 g,	↓The incidence of radiation pneumonia, ↓the incidence of bone marrow suppression, ↓C-reactive protein (CRP), ↑quality of life scale, ↑Karnofsky performance status (KPS), ↑total effective rates	Radiation pneumonia	Clinical study
Hu et al. [31]	Self-made Yangyin Qingfei decoction	Beishashen 10 g, Yuzhu 10 g, Maidong 15 g, Loquat leaf (Pipaye) 10 g, White mulberry bark (Sangbaipi) 12 g, Scutellariae (Huangqin) 15 g, Rhizoma anemarrhenae (Zhimu) 10 g, honeysuckle flower (Jinyinhua) 15 g, Forsythia (Lianqiao) 12 g, Zaoxiu 10 g, Hedyotis diffusa (Baihuashe shecao) 30 g, Gancao 6 g	↓Inflammatory response, ↑pulmonary function, ↑therapeutic effect	Radiation pneumonia	Clinical study
Liu and Wang [32]	Nourishing yin and nourishing lung decoction	Renshen 10 g, Biandou 10 g, Beishashen 15 g, Yuzhu 10 g, Maidong 15 g, Shizandra (Wuweizi) 9 g, Tianhuafen 15 g, Sangye 15 g, Pipaye 15 g, Xingren 10 g, Digupi 10 g, Gancao 6g	↓Malondialdehyde, (MDA), ↑superoxide dismutase (SOD), ↑total antioxidant capacity (T-AOC), ↑KPS, ↓prevalence of adverse reactions	Radiation pneumonia	Clinical observation study

Table 5: Continued.

Author	Name of drug or prescription	Formulation of the prescription	Major findings	Disease	Study types
Zhang et al. [33]	Self-made decoction	Huangqin 6 g, Reed rhizome (Lugen) 6 g, Chuanbei 6 g, Lianqiao 6 g, Gancao 6 g, Huangjing 10 g, Xuanshen 10 g, Aster (Ziwan) 10 g, Danggui 15 g, Baihe 10 g, Shengdi 15 g, Maidong 10 g, Sangbaipi 10 g, Herba houttuynia (Yuxingcao) 20 g, Beishashen 30 g, Shegan 10 g, Zicao 15 g, Tiandong 10 g, Yuzhu 10 g, Jiegeng 10 g, Paeonia lactiflora (Baishao) 30 g, North shashen 15 g	↑total effective rates, ↓prevalence of adverse reactions	Radiation pneumonia	Clinical study
Yun et al. [34]	Shashen Maidong decoction	Beishashen 15, Maidong 15, Sangye 10 g, Tianhuafeng 10 g, Biandou 10 g, Gancao 6 g	↑total effective rates, ↓TGF-β, ↓IL-6, ↓TNF-α, ↓severity classification of pneumonia	Radiation pneumonia	Clinical observation study
Wan et al. [35]	Shashen Maidong plus-minus decoction	Beishashen 30 g, Maidong 15 g, Yuzhu 10 g., Tianhuafeng 12 g, Sangye 10 g, Yuxingcao 10 g, Xingren 10 g, Jiegeng 10 g, Peony bark (Mudanpi) 10 g, Shengdihuang 15 g, Ligusticum chuanxiang (Chuanxiong) 10 g, Gancao 10 g	↓TNF-α, ↓CRP, ↓cough, ↓sputum, ↓urgent gas, ↓chest pain	Radiation pneumonia	Clinical observation study

5. Conclusions

To sum up, using network pharmacology, molecular docking, molecular dynamics, and big data information, our study investigated the probable mechanism of traditional marine Chinese medicine (Beishashen) in preventing and treating RILI and CILI. As a result of the regulation of the PI3K-AKT signaling pathway, as well as the involvement of the PTGS2 and RXRA gene expression, which may serve as the main potential mechanisms of action, various components of Beishashen serve as various targets for the prevention and treatment of RILI and CILI. This study offers not only a fresh look at the molecular mechanism of Beishashen for preventing and treating RILI and CILI, but it also serves as a foundation for contemporary pharmacology research in marine traditional Chinese medicine and even offers guidance for future experimental studies of RILI and CILI.

Data Availability

The data used in this study are available from the corresponding author upon reasonable request.

Disclosure

Bin Yu, Maoru Wang, and Lina Jia are the co-first authors.

Conflicts of Interest

All authors declare that they have no conflicts of interest.

Authors' Contributions

Bin Yu and Maoru Wang designed the study and wrote the manuscript. Hui Xu and Hong Ning supervised the study and revised the manuscript. Bin Yu, Lina Jia, and Yuanying Zhu collected the data and visualized the study. Yan Wu, Ting Luo, and Yubing Zhou analyzed the data. All authors reviewed the manuscript. Also, all authors have read and approved the final version of the manuscript. Bin Yu, Maoru Wang, and Lina Jia contributed equally to this work.

Acknowledgments

This study was supported by the NHC Key Laboratory of Nuclear Technology Medical Transformation (Mianyang Central Hospital) (Grant no. 2022HYX013), the Graduate Innovation Foundation (Nos. KGIFYTU2313 and KGIFYTU2221), and the Open Laboratory Project of Yantai University, China (2023).

References

[1] H. Sung, J. Ferlay, R. L. Siegel et al., "Global cancer statistics 2020: GLOBOCAN estimates of incidence and mortality worldwide for 36 cancers in 185 countries," *CA: A Cancer Journal for Clinicians*, vol. 71, no. 3, pp. 209–249, 2021.

[2] P. X. Zhou and S. X. Zhang, "Functional lung imaging in thoracic tumor radiotherapy: application and progress," *Frontiers Oncology*, vol. 12, Article ID 908345, 2022.

[3] A. M. Atwa, O. A. M. Abd El-Ghafar, E. H. M. Hassanein et al., "Candesartan attenuates cisplatin-induced lung injury by modulating oxidative stress, inflammation, and TLR-4/NF-κB, JAK1/STAT3, and Nrf2/HO-1 signaling," *Pharmaceuticals*, vol. 15, no. 10, pp. 1222–2022, 2022.

[4] D. Jornet, P. Loap, J. Y. Pierga et al., "Neoadjuvant concurrent radiotherapy and chemotherapy in early breast cancer patients: long-term results of a prospective phase II trial," *Cancers*, vol. 13, no. 20, Article ID 5107, 2021.

[5] R. P. Abratt and G. W. Morgan, "Lung toxicity following chest irradiation in patients with lung cancer," *Lung Cancer*, vol. 35, no. 2, pp. 103–109, 2002.

[6] M. F. Benveniste, J. Welsh, M. C. Godoy, S. L. Betancourt, O. R. Mawlawi, and R. F. Munden, "New era of radiotherapy: an update in radiation-induced lung disease," *Clinical Radiology*, vol. 68, no. 6, pp. e275–e290, 2013.

[7] S. Bian, H. Cai, Y. Cui, W. Liu, and C. Xiao, "Nanomedicine-based therapeutics to combat acute lung injury," *International Journal of Nanomedicine*, vol. 16, pp. 2247–2269, 2021.

[8] L. Knudsen, E. Lopez-Rodriguez, L. Berndt et al., "Alveolar micromechanics in bleomycin-induced lung injury," *American Journal of Respiratory Cell and Molecular Biology*, vol. 59, no. 6, pp. 757–769, 2018.

[9] E. K. Incerpi, L. M. Oliveira, E. M. Pereira, and R. Soncini, "Inhibition of endogenous glucocorticoid synthesis aggravates lung injury triggered by septic shock in rats," *International Journal of Experimental Pathology*, vol. 96, no. 3, pp. 133–139, 2015.

[10] M. L. Hensley, K. L. Hagerty, T. Kewalramani et al., "American society of clinical oncology 2008 clinical practice guideline update: use of chemotherapy and radiation therapy protectants," *Journal of Clinical Oncology*, vol. 27, no. 1, pp. 127–145, 2009.

[11] M. I. Koukourakis, M. Panteliadou, I. M. Abatzoglou, K. Sismanidou, E. Sivridis, and A. Giatromanolaki, "Post-mastectomy hypofractionated and accelerated radiation therapy with (and without) subcutaneous amifostine cytoprotection," *International Journal of Radiation Oncology, Biology, Physics*, vol. 85, no. 1, pp. e7–e13, 2013.

[12] Y. T. Ma, Y. P. Tian, H. W. Shi, C. H. Lv, J. H. Liu, and Z. P. Sun, "Effects of high dose ambroxol on lung injury induced by paraquat in rats," *Zhonghua Lao Dong Wei Sheng Zhi Ye Bing Za Zhi*, vol. 25, no. 9, pp. 523–526, 2007.

[13] C. Tabata, Y. Kadokawa, R. Tabata et al., "All-trans-retinoic acid prevents radiation- or bleomycin-induced pulmonary fibrosis," *American Journal of Respiratory and Critical Care Medicine*, vol. 174, no. 12, pp. 1352–1360, 2006.

[14] X. Zhu, Y. Zhang, X. Liu, D. Hou, and T. Gao, "Authentication of commercial processed glehniae radix (beishashen) by DNA barcodes," *Chinese Medicine*, vol. 10, no. 1, p. 35, 2015.

[15] J. Rozema, P. Bijwaard, G. Prast, and R. Broekman, "Ecophysiological adaptations of coastal halophytes from foredunes and salt marshes," *Vegetatio*, vol. 62, no. 1-3, pp. 499–521, 1985.

[16] H. Matsuura, G. Saxena, S. W. Farmer, R. E. Hancock, and G. Towers, "Antibacterial and antifungal polyine compounds from*Glehnia littoralis*ssp.*leiocarpa*," *Planta Medica*, vol. 62, no. 3, pp. 256–259, 1996.

[17] J. H. Park, T. K. Lee, B. C. Yan et al., "Pretreated glehnia littoralis extract prevents neuronal death following transient global cerebral ischemia through increases of superoxide dismutase 1 and brain-derived neurotrophic factor expressions in the gerbil hippocampal cornu ammonis 1 area," *Chinese Medical Journal*, vol. 130, no. 15, pp. 1796–1803, 2017.

[18] J. Wu, W. Gao, Z. Song et al., "Anticancer activity of polysaccharide from Glehnia littoralis on human lung cancer cell line A549," *International Journal of Biological Macromolecules*, vol. 106, pp. 464–472, 2018.

[19] T. Yoon, D. Y. Lee, A. Y. Lee, G. Choi, B. K. Choo, and H. K. Kim, "Anti-inflammatory effects of glehnia littoralis extract in acute and chronic cutaneous inflammation," *Immunopharmacology and Immunotoxicology*, vol. 32, no. 4, pp. 663–670, 2010.

[20] Y. Y. Lian, Y. X. Wan, L. L. Li et al., "Exploring the medication rules and action mechanism for treating radiationinduced lung injury based on data mining and network pharmacology," *Modern Chinese Clinical Medicine*, vol. 29, no. 6, pp. 64–70, 2022.

[21] S. Guo, Y. Li, H. Su et al., "Aidi injection as adjunctive treatment to gemcitabine-based chemotherapy for advanced non-small cell lung cancer: a systematic review and meta-analysis," *Pharmaceutical Biology*, vol. 59, no. 1, pp. 1258–1273, 2021.

[22] C. Yang, C. Song, Y. Wang et al., "Re-Du-Ning injection ameliorates radiation-induced pneumonitis and fibrosis by inhibiting AIM2 inflammasome and epithelial-mesenchymal transition," *Phytomedicine*, vol. 102, Article ID 154184, 2022.

[23] M. Wang, B. Yu, J. Wang, Y. Wang, and L. Liang, "Exploring the role of Xingren on COVID-19 based on network pharmacology and molecular docking," *Journal of Food Biochemistry*, vol. 46, no. 10, Article ID e14363, 2022.

[24] X. Ruan, P. Du, K. Zhao et al., "Mechanism of Dayuanyin in the treatment of coronavirus disease 2019 based on network pharmacology and molecular docking," *Chinese Medicine*, vol. 15, no. 1, p. 62, 2020.

[25] M. Qasim, M. Abdullah, U. Ali Ashfaq et al., "Molecular mechanism of Ferula asafoetida for the treatment of asthma: network pharmacology and molecular docking approach," *Saudi Journal of Biological Sciences*, vol. 30, no. 2, Article ID 103527, 2023.

[26] Y. Yang and Y. Zhou, "Shashen-Maidong decoction-mediated IFN-γ and IL-4 on the regulation of Th1/Th2 imbalance in RP rats," *BioMed Research International*, vol. 2019, Article ID 6012473, pp. 1–7, 2019.

[27] R. Z. Qi, Y. Y. Yang, J. G. Liu, X. W. Wu, and B. J. Hua, "Pathological changes of lung tissue and the semi-quantitative analysis of alveolar inflammation of rats in the model of acute radiation induced lung injury treated with Shashen Jiegeng Decoction," *China Journal of Traditional Chinese Medicine and Pharmacy*, vol. 35, no. 2, pp. 616–619, 2021.

[28] K. Wu, X. H. Peng, W. Zhu, and M. L. Min, "Clinical study on the prevention and treatment of PD-1 inhibitor-related lung injury by Shashen Maidong Decoction," *YUNNAN JOURNAL OF TRADITIONAL CHINESE MEDICINE AND MATERIA MEDICA*, vol. 43, no. 1, pp. 50–52, 2022.

[29] Q. B. Wu, C. F. Feng, D. K. Zhu, and Y. Luo, "Clinical observation on Shashen Jiegeng Decoction combined with prednisolone on radiation pneumonia," *Journal of Hubei University of Chinese Medicine*, vol. 23, no. 3, pp. 18–21, 2021.

[30] X. Li, J. Huang, J. Luo, D. M. Pan, Q. Long, and L. Ren, "Clinical effect of shashen maidong decoction on prevention and treatment of radiation pneumonia," *World Journal of Complex Medicine*, vol. 9, no. 6, pp. 1–4+8, 2023.

[31] Z. W. Hu, X. J. Gu, Y. Jiang, and T. Duan, "Curative effect of acupuncture combined with the method for nourishing Yin and detoxification on radiation pneumonia and its effect on serum IL-6, TGF-β1 and CRP," *Modern Journal of Integrated Traditional Chinese and Western Medicine*, vol. 30, no. 20, pp. 3344–3348, 2021.

[32] C. Liu and Y. M. Wang, "Observation on clinical efficacy of nourishing yin and nourishing lung combined with acupoint application in the prevention and treatment of radiation pneumonia (qi and yin deficiency syndrome)," *Guiding Journal of Traditional Chinese Medicine and Pharmacology*, vol. 27, no. 3, pp. 79–82, 2021.

[33] Y. T. Zhang, C. C. Wang, F. Huang, and X. M. Qu, "Study on the clinical treatment of acute radiation pneumonia caused by radiotherapy of lung cancer," *Chinese General Practice*, vol. 24, no. S1, pp. 103–105, 2021.

[34] Y. Yun, S. S. Li, S. D. Shi et al., "Clinical observation of shashen maidong decoction combined with western medicine in the treatment of radiation pneumonia," *CLINICAL JOURNAL OF TRADITIONAL CHINESE MEDICINE*, vol. 34, no. 6, pp. 1109–1112, 2022.

[35] X. F. Wan, F. J. He, and X. Y. Du, "Clinical observation on 46 cases of acute radiation pneumonitis after radiotherapy for lung cancer treated with western medicine combined with Shashen maidong plus-minus decoction," *Chinese Journal of Ethnomedicine and Ethnopharmacy*, vol. 30, no. 17, pp. 107–109, 2021.

[36] J. Peng, X. Chen, M. Hou et al., "The TCM preparation feilike mixture for the treatment of pneumonia: network analysis, pharmacological assessment and silico simulation," *Frontiers in Pharmacology*, vol. 13, Article ID 794405, 2022.

[37] X. Tang, H. Zhao, W. Jiang et al., "Pharmacokinetics and pharmacodynamics of citrus peel extract in lipopolysaccharide-induced acute lung injury combined with Pinelliae Rhizoma Praeparatum," *Food & Function*, vol. 9, no. 11, pp. 5880–5890, 2018.

[38] N. O. El-Shaer, A. M. Hegazy, and M. H. Muhammad, "Protective effect of quercetin on pulmonary dysfunction in streptozotocin-induced diabetic rats via inhibition of NLRP3 signaling pathway," *Environmental Science and Pollution Research*, vol. 30, no. 14, pp. 42390–42398, 2023.

[39] J. Wang, Y. Y. Zhang, J. Cheng, J. L. Zhang, and B. S. Li, "Preventive and therapeutic effects of quercetin on experimental radiation induced lung injury in mice," *Asian Pacific Journal of Cancer Prevention*, vol. 16, no. 7, pp. 2909–2914, 2015.

[40] H. Liu, J. X. Xue, X. Li, R. Ao, and Y. Lu, "Quercetin liposomes protect against radiation-induced pulmonary injury in a murine model," *Oncology Letters*, vol. 6, no. 2, pp. 453–459, 2013.

[41] S. Verma, A. Dutta, A. Dahiya, and N. Kalra, "Quercetin-3-Rutinoside alleviates radiation-induced lung inflammation and fibrosis via regulation of NF-κB/TGF-β1 signaling," *Phytomedicine*, vol. 99, Article ID 154004, 2022.

[42] X. F. Wang, S. D. Song, Y. J. Li et al., "Protective effect of quercetin in LPS-induced murine acute lung injury mediated by cAMP-Epac pathway," *Inflammation*, vol. 41, no. 3, pp. 1093–1103, 2018.

[43] Q. Lv, P. Zhang, P. Quan et al., "Quercetin, a pneumolysin inhibitor, protects mice against Streptococcus pneumoniae infection," *Microbial Pathogenesis*, vol. 140, Article ID 103934, 2020.

[44] N. P. da Silva Araújo, N. A. de Matos, S. Leticia Antunes Mota et al., "Quercetin attenuates acute lung injury caused by cigarette smoke both in vitro and in vivo," *COPD: Journal of Chronic Obstructive Pulmonary Disease*, vol. 17, no. 2, pp. 205–214, 2020.

[45] P. Maturu, Y. Wei-Liang, V. P. Androutsopoulos et al., "Quercetin attenuates the hyperoxic lung injury in neonatal mice: implications for Bronchopulmonary dysplasia (BPD)," *Food and Chemical Toxicology*, vol. 114, pp. 23–33, 2018.

[46] J. A. Martinez, S. G. Ramos, M. S. Meirelles, A. V. Verceze, M. R. Arantes, and H. Vannucchi, "Efeitos da quercetina na lesão pulmonar induzida por bleomicina: um estudo preliminar," *Jornal Brasileiro de Pneumologia*, vol. 34, no. 7, pp. 445–452, 2008.

[47] H. K. Park, S. J. Kim, D. Y. Kwon, J. H. Park, and Y. C. Kim, "Protective effect of quercetin against paraquat-induced lung injury in rats," *Life Sciences*, vol. 87, no. 5-6, pp. 181–186, 2010.

[48] X. Lai and M. Najafi, "Redox interactions in chemo/radiation therapy-induced lung toxicity; mechanisms and therapy perspectives," *Current Drug Targets*, vol. 23, no. 13, pp. 1261–1276, 2022.

[49] S. Drishya, S. S. Dhanisha, P. Raghukumar, and C. Guruvayoorappan, "Amomum subulatum mitigates experimental thoracic radiation-induced lung injury by regulating antioxidant status and inflammatory responses," *Food & Function*, vol. 14, no. 3, pp. 1545–1559, 2023.

[50] C. Li, E. Changyong, Y. Zhou, and W. Yu, "Candidate genes and potential mechanisms for chemoradiotherapy sensitivity in locally advanced rectal cancer," *Oncology Letters*, vol. 17, no. 5, pp. 4494–4504, 2019.

[51] X. Z. Zhang, M. J. Chen, P. M. Fan, T. S. Su, S. X. Liang, and W. Jiang, "Prediction of the mechanism of sodium butyrate against radiation-induced lung injury in non-small cell lung cancer based on network pharmacology and molecular dynamic simulations and molecular dynamic simulations," *Frontiers Oncology*, vol. 12, Article ID 809772, 2022.

[52] G. Gong, K. Ganesan, Q. Xiong, and Y. Zheng, "Antitumor effects of ononin by modulation of apoptosis in non-small-cell lung cancer through inhibiting PI3K/Akt/mTOR pathway," *Oxidative Medicine and Cellular Longevity*, vol. 2022, Article ID 5122448, pp. 1–17, 2022.

[53] Y. Tang, B. Liu, J. Li et al., "Genetic variants in PI3K/AKT pathway are associated with severe radiation pneumonitis in lung cancer patients treated with radiation therapy," *Cancer Medicine*, vol. 5, no. 1, pp. 24–32, 2016.

[54] A. Arora, V. Bhuria, S. Singh et al., "Amifostine analog, DRDE-30, alleviates radiation induced lung damage by attenuating inflammation and fibrosis," *Life Sciences*, vol. 298, Article ID 120518, 2022.

[55] Y. Xu, Y. Huang, Y. Chen et al., "Grape seed proanthocyanidins play the roles of radioprotection on normal lung and radiosensitization on lung cancer via differential regulation of the MAPK signaling pathway," *Journal of Cancer*, vol. 12, no. 10, pp. 2844–2854, 2021.

[56] D. Y. Zhao, H. J. Qu, J. M. Guo et al., "Protective effects of myrtol standardized against radiation-induced lung injury," *Cellular Physiology and Biochemistry*, vol. 38, no. 2, pp. 619–634, 2016.